Inorganic Chemistry

Article

pubs.acs.org/IC

Comparative Study of C^N and N^C Type Cyclometalated Ruthenium Complexes with a NAD$^+$/NADH Function

Sumanta Kumar Padhi,[†] Ryoichi Fukuda,[§] Masahiro Ehara,[§] and Koji Tanaka*[,†,‡]

[†]Department of Life and Coordination-Complex Molecular Science, Institute for Molecular Science, 5-1, Higashiyama, Myodaiji, Okazaki, Aichi 444-8787, Japan

[‡]Institute for Integrated Cell-Material Sciences, Kyoto University, Funai Center #201, Kyoto University Katsura, Nishikyo-ku, Kyoto 615-8530, Japan

[§]Department of Theoretical and Computational Molecular Science, Institute for Molecular Science and Research Center for Computational Science, 38 Nishigo-Naka, Myodaiji, Okazaki 444-8585, Japan

S *Supporting Information*

ABSTRACT: Cyclometalated ruthenium complexes having C^N and N^C type coordinating ligands with NAD$^+$/NADH function have been synthesized and characterized by spectroscopic methods. The variation of the coordinating position of σ-donating carbon atom leads to a drastic change in their properties. Both the complex Ru(**phbn**)(phen)$_2$]PF$_6$ ([**1**]PF$_6$) and [Ru(**pad**)(phen)$_2$]PF$_6$ ([**2**]PF$_6$) reduced to Ru(**phbnHH**)(phen)$_2$]PF$_6$ ([**1HH**]PF$_6$) and [Ru(**padHH**)-(phen)$_2$]PF$_6$ ([**2HH**]PF$_6$) by chemical and electrochemical methods. Complex [**1**]PF$_6$ photochemically reduced to [**1HH**]PF$_6$ in the presence of the sacrificial agent triethylamine (TEA) upon irradiation of visible light ($\lambda \geq 420$ nm), whereas photochemical reduction of [**2**]PF$_6$ was not successful. Both experimental results and theoretical calculations reveal that upon protonation the energy level of the π^* orbital of either of the ligands **phbn** or **pad** is drastically stabilized compared to the nonprotonated forms. In the protonated complex [Ru(**padH**)(phen)$_2$](PF$_6$)$_2$ {[**2H**](PF$_6$)$_2$}, the Ru−C bond exists in a tautomeric equilibrium with Ru═C coordination and behaves as a remote N-heterocyclic carbene (*r*NHC) compex; on the contrary, this behavior could not be observed in protonated complex [Ru(**phbnH**)(phen)$_2$](PF$_6$)$_2$ {[**1H**](PF$_6$)$_2$}.

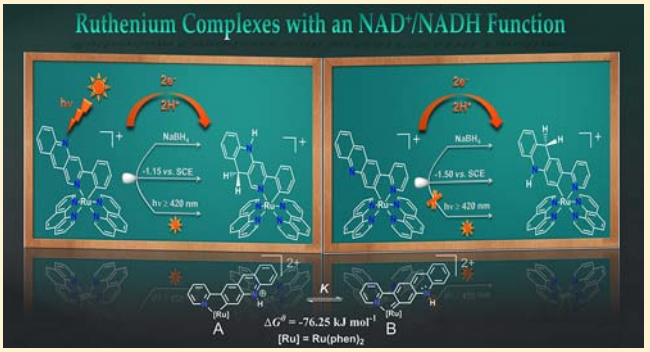

INTRODUCTION

In natural photosynthesis, light-dependent reactions capture the energy of light that is used to compose the energy-storage molecules ATP and NADPH.[1] The electrons and protons taken from water using solar energy reduces NAD(P)$^+$, generating the 1,4-dihydro form NAD(P)H, which is used to reductively fix CO_2 as carbohydrates through the Calvin cycle.[2] The bioactive coenzyme nicotinamide adenine dinucleotide (NAD$^+$) functions as a two electron and a proton acceptor to generate dihydronicotinamide adenine dinucleotide (NADH) as outlined in Scheme 1. With the subsequent release of hydride from NADH, it converts to NAD$^+$ in a reversible pathway.[3]

Scheme 1. NAD$^+$/NADH Redox Behavior

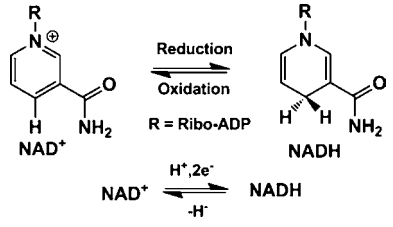

For a decade, extensive efforts have been devoted for the functional mimic of NAD$^+$/NADH model in ruthenium polypyridine complexes (Scheme 2) through chemical, electrochemical, and photochemical methods.[4] The electrochemical reduction of (**a**) at −1.34 V (vs Fc/Fc$^+$) in H_2O results in bond formation between the noncoordinating N atom of napy (napy = 1,8-naphthyridine) and the carbonyl carbon atom with the subsequent hydrogenation of the napy ring to form (**a′**).[4m] The oxidation of (**a′**) at 0.06 V regenerated (**a**) reversibly, where the formation of a C−H bond in the pyridinium ring occurs with two electrons and one proton. The complex (**b′**) was produced with the reduction of corresponding carbonyl complex (**b**) at −0.95 V (vs Ag/Ag$^+$).[4i] Complexes (**c**) and (**d**) under controlled potential electrolysis at −1.14 V (vs Fc/Fc$^+$) produces the respective reduced forms (**c′**) and (**d′**).[4b−d,l] Among these homoleptic coordinated complexes, (**c**) {R = H} and (**d**) undergo photochemical reduction upon continuous photolysis of the respective CH_3CN solution in the presence of sacrificial agents like TEA or TEOA.

Received: February 28, 2012
Published: July 24, 2012

dx.doi.org/10.1021/ic300449q | *Inorg. Chem.* 2012, 51, 8091−8102

Scheme 2. NAD$^+$/NADH Model Ruthenium Complexes

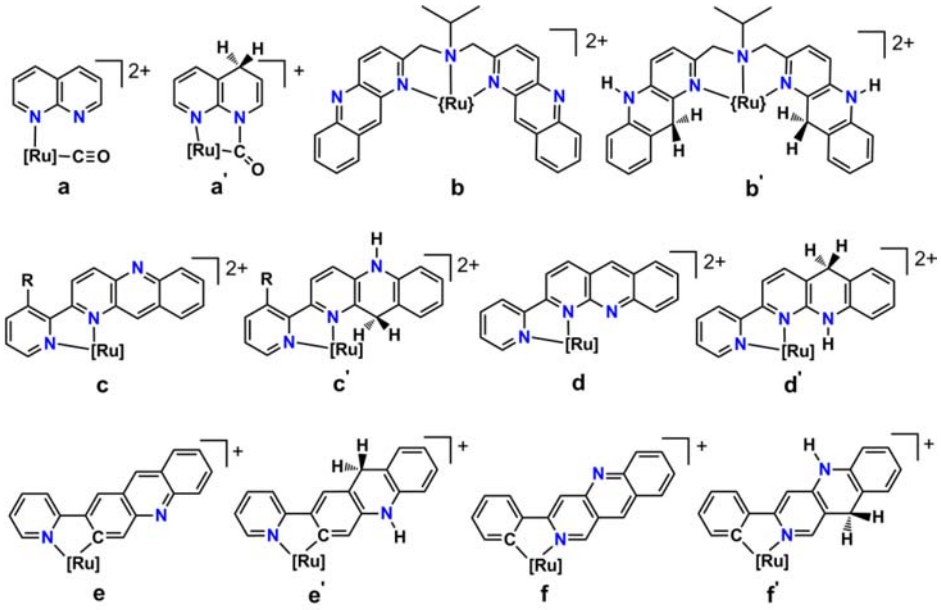

The heteroleptically coordinated N^C and C^N type cyclometalated complexes (**e**) and (**f**) also reduced to (**e**′) and (**f**′), respectively, by chemical and electro-chemical methods [at −1.5 V {complex (**e**)} and −1.15 V {complex (**f**)} vs SCE].[5] Complex (**f**) photochemically reduced to (**f**′),[5a] whereas (**e**) does not undergo photodriven hydrogenation reaction.[5b]

The most interesting behavior of complex (**e**) is the remote N-heterocyclic carbene (*r*NHC) type behavior after protonation at the noncoordinated nitrogen atom. Reports on "nonclassical" NHCs are very rare.[6] It was the first acridine-based ruthenium *r*NHC complex with no hetero atoms in the carbene containing ring because the nitrogen atom is located in an adjacent annealed aromatic ring (Scheme 3).[5b] Usually

Scheme 3. Tautomeric Equilibrium in [Ru(padH)(bpy)$_2$]$^{2+}$

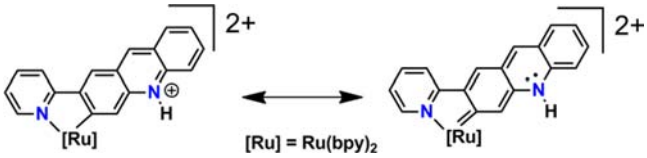

the σ-donating and π-accepting abilities of pyridine-based *r*NHCs are stronger than that of general imidazole-2-ylidines.[7] Metal-induced rearrangements in some pyridines generates NHC ligands that involve tautomerization processes have been reported by the Bergman, Carmona, and Esteruelas groups.[8]

In the present study, we demonstrate a comparison of detailed spectroscopic studies for the ruthenium complexes having C^N and N^C type cyclometalated ligands with an NAD$^+$/NADH function.

RESULTS AND DISCUSSION

Synthesis. The ligands 3-phenylbenzo[b][1,6]-naphthyridine (**phbn**), 2-(pyridin-2-yl)acridine (**pad**), and 2-(pyridin-2-yl)-9,10-dihydroacridine (**padHH**) were prepared according to the literature procedure.[5] The precursor complexes [Ru(**phbn**)(CH$_3$CN)$_4$]PF$_6$ and [Ru(**pad**)(CH$_3$CN)$_4$]-PF$_6$ were synthesized following the reported procedure.[5] Further addition of two equivalents of 1,10-phenanthroline (phen) with either [Ru(**phbn**)(CH$_3$CN)$_4$]PF$_6$ or [Ru(**pad**)-(CH$_3$CN)$_4$]PF$_6$ in 2-methoxyethanol, respectively, affords the corresponding *bis*-(1,10-phenanthroline) complexes [Ru-(**phbn**)(phen)$_2$]PF$_6$ ([**1**]PF$_6$) and [Ru(**pad**)(phen)$_2$]PF$_6$ ([**2**]PF$_6$). The details of the complex syntheses are outlined in Schemes 4 and 5. Both the complexes [**1**]PF$_6$ and [**2**]PF$_6$

Scheme 4. Synthesis of Complexes [1], [1H]$^{2+}$, and [1HH]$^+$

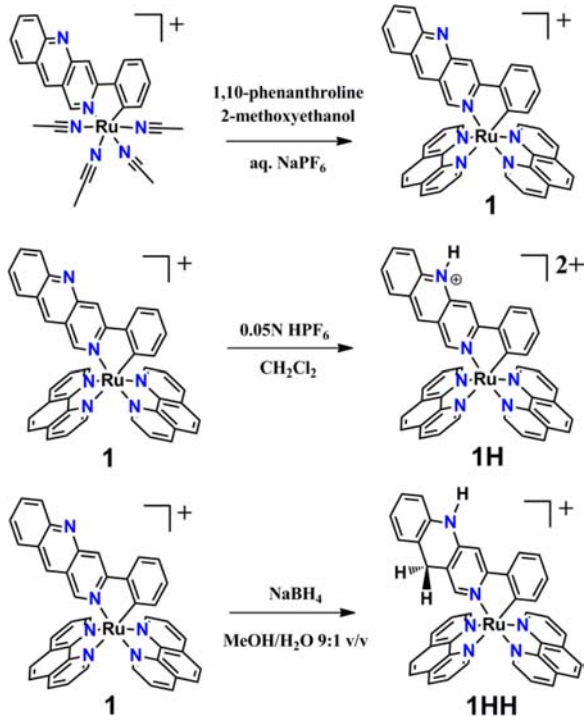

possess a noncoordinating nitrogen that is susceptible toward protonation. With the dropwise addition of 0.05N HPF$_6$ into a

dx.doi.org/10.1021/ic300449q | Inorg. Chem. 2012, 51, 8091−8102

Scheme 5. Synthesis of Complexes [2], $[2H]^{2+}$, and $[2HH]^{+}$

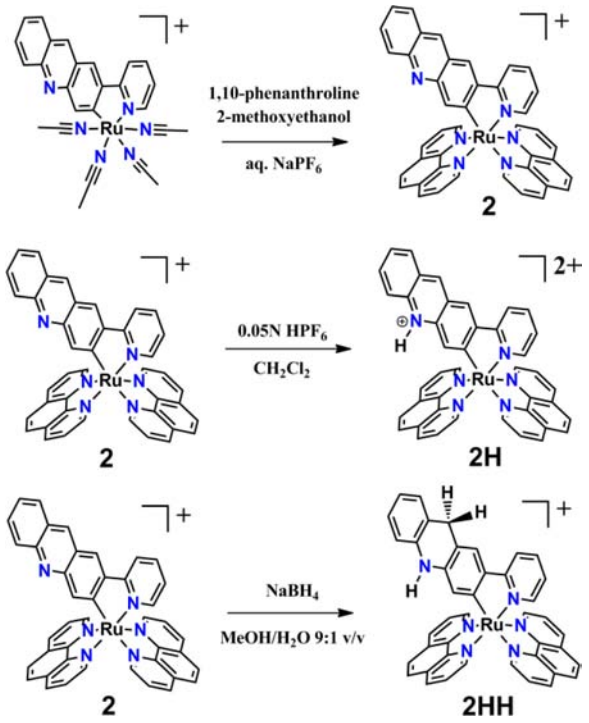

dichlomethane solution of the complex $[1]PF_6$ or $[2]PF_6$, the respective protonated complexes $[1H](PF_6)_2$ (orange color) and $[2H](PF_6)_2$ (green color) were isolated.

Complex $[1]PF_6$ was reduced to $[Ru(\mathbf{phbnHH})(phen)_2]PF_6$ ($[1HH]PF_6$) by chemical, electrochemical, and photochemical methods. By the treatment of $[1]PF_6$ with $NaBH_4$ in a methanol/H_2O mixture (9:1 v/v) under nitrogen atmosphere, $[1HH]PF_6$ was isolated in a very good yield of (87%). The purple color of $[1]PF_6$ gradually turned to pink under the controlled potential electrolysis at −1.10 V (vs SCE) in CH_3CN/H_2O (9:1 v/v) containing Bu_4NPF_6 as a supporting electrolyte (0.1 M), and $[1HH]PF_6$ was produced after consumption of two equivalent of electrons in the electrolysis. The ^1H NMR, cyclic voltammogram, and the UV−vis spectra of the resultant product were consistent with those of $[1HH]PF_6$ obtained by the chemical reduction method (vide infra). The ^1H NMR spectrum (Figure 1) of $[1HH]PF_6$ in

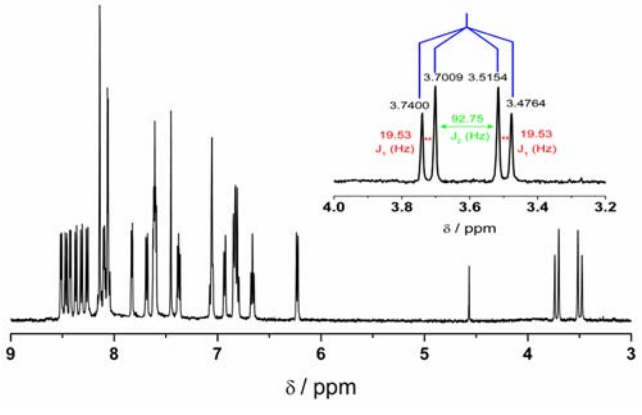

Figure 1. ^1H NMR of $[1HH]PF_6$ in CD_3CN at 293 K.

CD_3CN displayed 20 different signals with a total intensity of 29 protons, out of which 26 are in the aromatic region generating from two phen and **phbnHH** ligand, and the NH proton appears at 4.57 ppm. An AB patterned doublet was observed at 3.50 {1H, d, (J, H_z) = 19.53} and 3.72 {1H, d, (J, H_z) = 19.53} ppm due to the geminal coupling of the methylene protons. The methylene carbon appeared at 28.0 ppm in ^{13}C NMR.

The complex $[2]PF_6$ was reduced to $[2HH]PF_6$ by both the chemical as well as the electrochemical method. It could not be successful by the photochemical method with the presence of sacrificial reagents like triethyl amine (TEA) or triethanolamine (TEOA). Under the controlled potential electrolysis at −1.5 V (vs SCE) in CH_3CN/H_2O (9:1 (v/v)) containing Bu_4NPF_6 as a supporting electrolyte (0.1 M), the red color of $[2]PF_6$ gradually turned to dark red, and $[2HH]PF_6$ was produced after consumption of two equivalent of electrons during electrolysis. The NMR, cyclic voltammogram, and UV−vis spectra of the final product were consistent with those of $[2HH]PF_6$ obtained by the treatment of $[2]PF_6$ with $NaBH_4$ in a methanol/H_2O mixture (9:1 v/v) under nitrogen atmosphere. The ^1H NMR spectrum of $[2HH]PF_6$ in CD_3CN (Figure 2) displayed 17

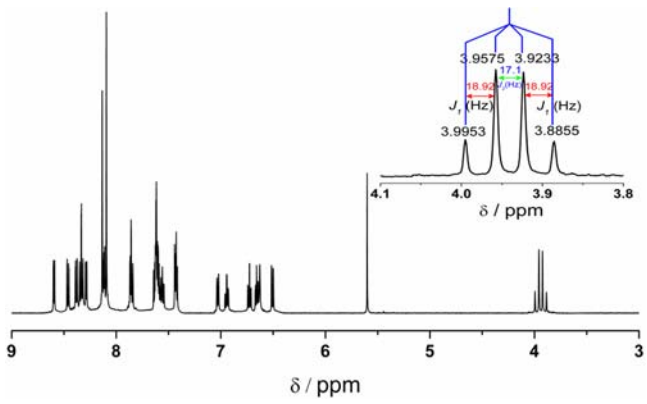

Figure 2. ^1H NMR of $[2HH]PF_6$ in CD_3CN at 293 K.

different signals with a total intensity of 29 protons, out of which 26 are in the aromatic region arising from two phen and the **padHH** ligand. The NH proton peak appeared at δ = 5.60 ppm, and an AB patterned doublet was observed at 3.91 {1H, d, (J, H_z) = 18.92} and 3.98 {1H, d, (J, H_z) = 18.92} ppm by the methylene protons due to the geminal coupling. The ^{13}C NMR of the methylene carbon appears at 31.64 ppm.

Optical Properties. In the visible region, 400−600 nm, each of these prescribed complexes exhibit the CT bands. The intraligand charge transfer (ILCT) peaks appeared in the UV region 250−280 nm are of n→π^* origin (Figure S13, Supporting Information), and the $\pi\rightarrow\pi^*$ transitions occur in the 285−375 nm region. Under protic conditions, the UV−vis spectra of $[1]PF_6$ shows a bathochromic shift in the CT absorption band from 540 to 740 nm on the basis of the **phbn** ligand as the color changes from purple to orange. It causes a decrease in energy of the π^* orbital in **phbn** after protonation resulting in a red shift. The pK_a of $[1H]^{2+}$ was determined to be 3.91 from the pH dependent UV−vis spectra in aqueous solution (Figure S20, Supporting Information). The complex $[1HH]PF_6$ exhibits a CT band at λ_{max} = 550 nm. Complex $[2]PF_6$ shows the CT band at 525 nm, and upon protonation, the bathochromic shift was observed at 640 nm. From the pH

dx.doi.org/10.1021/ic300449q | Inorg. Chem. 2012, 51, 8091−8102

Table 1. Electronic and Emission Spectral Data[a]

complexes	λ_{abs} (nm)	$\varepsilon_{max} \times 10^{-4}$ (M^{-1} cm^{-1})	λ_{em} (nm)	λ_{ex} (nm)	Φ	reference
$[Ru(\mathbf{phbn})(phen)_2]^+$	540	1.20	770	540	0.005	this work
$[Ru(\mathbf{phbnH})(phen)_2]^{2+}$	740	0.16	850	750	0.003	this work
$[Ru(\mathbf{phbnHH})(phen)_2]^+$	550	0.88	770	540	0.005	this work
$[Ru(\mathbf{phbn})(bpy)_2]^+$	550	1.30	860	550	0.005	5a
$[Ru(\mathbf{phbnH})(bpy)_2]^{2+}$	750	0.15	845	750	0.004	this work
$[Ru(\mathbf{phbnHH})(bpy)_2]^+$	565	1.10	865	550	0.006	5a
$[Ru(\mathbf{pad})(phen)_2]^+$	525	1.20	730, 870	450, 530	0.007	this work
$[Ru(\mathbf{padH})(phen)_2]^{2+}$	640	0.54	830	650	0.006	this work
$[Ru(\mathbf{padHH})(phen)_2]^+$	525	1.10	730, 870	450, 530	0.007	this work
$[Ru(\mathbf{pad})(bpy)_2]^+$	530	0.78	750	535	0.003	5a
$[Ru(\mathbf{padH})(bpy)_2]^{2+}$	650	0.53	825	650	0.004	this work
$[Ru(\mathbf{padHH})(bpy)_2]^+$	550	1.00	750	550	0.003	this work

[a]All the spectra were recorded in CH_3CN at 293 K.

Table 2. TDDFT Results

state	EE[a] (eV)	Abs[b] (nm)	Osc[c]	transition and amplitude[d]
$[\mathbf{1}]^+$				
1^1A	2.03	610	0.000	0.59 ($H^e \rightarrow L^f$)
2^1A	2.12	586	0.008	0.56 (H→L+3)
3^1A	2.29	542	0.023	0.64 (H→L+1)
$[\mathbf{1H}]^{2+}$				
1^1A	1.18	1054	0.091	0.68 (H→L)
2^1A	1.36	915	0.000	0.70 (H−1→L)
3^1A	1.68	738	0.065	0.68 (H−2→L)
$[\mathbf{1HH}]^+$				
1^1A	2.04	608	0.000	0.62 (H→L)
7^1A	2.47	502	0.069	0.40 (H−2→L) − 0.32 (H−1→L)
8^1A	2.56	485	0.079	0.39 (H−1→L+1) − 0.33 (H−2→L+2)
$[\mathbf{2}]^+$				
1^1A	2.02	615	0.001	0.62 (H→L)
7^1A	2.57	482	0.055	0.34 (H−2→L) + 0.31(H−3→L)
$[\mathbf{2H}]^{2+}$				
1^1A	2.19	565	0.027	0.55 (H−1→L) − 0.42 (H→L)
2^1A	2.32	535	0.116	0.44 (H→L) + 0.39(H−1→L)
$[\mathbf{2HH}]^{2+}$				
1^1A	1.89	655	0.004	0.65 (H→L)
11^1A	2.60	477	0.108	0.44 (H−3→L) + 0.32(H−2→L+1)

[a]Excitation energy. [b]Absorption wavelength. [c]Oscillator strength. [d]Amplitude and orbital transition in parentheses. [e]HOMO. [f]LUMO.

dependent UV−vis spectra in aqueous solution, the pK_a of $[\mathbf{2H}]^{2+}$ was determined to be 8.81 (Figure S21, Supporting Information). The reduced complex has the λ_{max} at 525 nm, attributed to the CT band.

All the complexes $[\mathbf{1}]PF_6$, $[\mathbf{1H}](PF_6)_2$, $[\mathbf{1HH}]PF_6$, $[\mathbf{2}]PF_6$, $[\mathbf{2H}](PF_6)_2$, and $[\mathbf{2HH}]PF_6$ exhibit emission spectra (Figures S14−S19, Supporting Information). The complex $[\mathbf{1}]PF_6$ displays emission spectra at 770 nm upon excitation at 540 nm (Table 1). The protonated complex $[\mathbf{1H}](PF_6)_2$ has the emission maximum at 850 nm (λ_{ex} at 750 nm). Complex $[\mathbf{1HH}]PF_6$ shows the emission band at 770 nm exciting at 540 nm. In complex $[\mathbf{2}]PF_6$, two emission bands were observed at 730 and 870 nm, respectively, with the excitation at 450 and 530 nm. In $[\mathbf{2H}](PF_6)_2$, the emission maximum appears at 830 nm (λ_{ex} at 650 nm). The reduced complex $[\mathbf{2HH}]PF_6$ has the similar emissive behavior like $[\mathbf{2}]PF_6$, where two emission bands were observed at 730 and 870 nm with excitation at 450 and 530 nm, respectively. The quantum yields (**Φ**) for all these complexes were calculated with respect to the reference standard $[Ru(bpy)_3](PF_6)_2$.

Electronic Transitions and Computational Study. The complete lists of optimized atomic coordinates are shown in the Supporting Information. The Ru−C bond length of complex $[\mathbf{2}]^+$ is shortened by the protonation for **pad** as expected from eq 2 for the tautomer B (vide infra). The calculated Ru−C distance is 2.045 Å for $[\mathbf{2}]^+$ and that is 2.016 (Å) for $[\mathbf{2H}]^{2+}$ (Table S1, Supporting Information). The Ru−C distance of $[\mathbf{2HH}]^+$ is 2.048 Å. The reduced ligands **phbnHH** and **padHH** have nonplanar structure. The tricyclic unit was bent on the axis between nitrogen and reduced carbon atoms. The out-of-plane angle is about 20 degree.

The selected excited states obtained by TDDFT calculations are shown in Table 2. The details of TDDFT results are summarized in Tables S2−S7 of the Supporting Information with the isosurface plots of the Kohn−Sham molecular orbitals (MOs) that are relevant to the electronic excitations. The simulated absorption spectra by the TDDFT calculations are

dx.doi.org/10.1021/ic300449q | Inorg. Chem. 2012, 51, 8091−8102

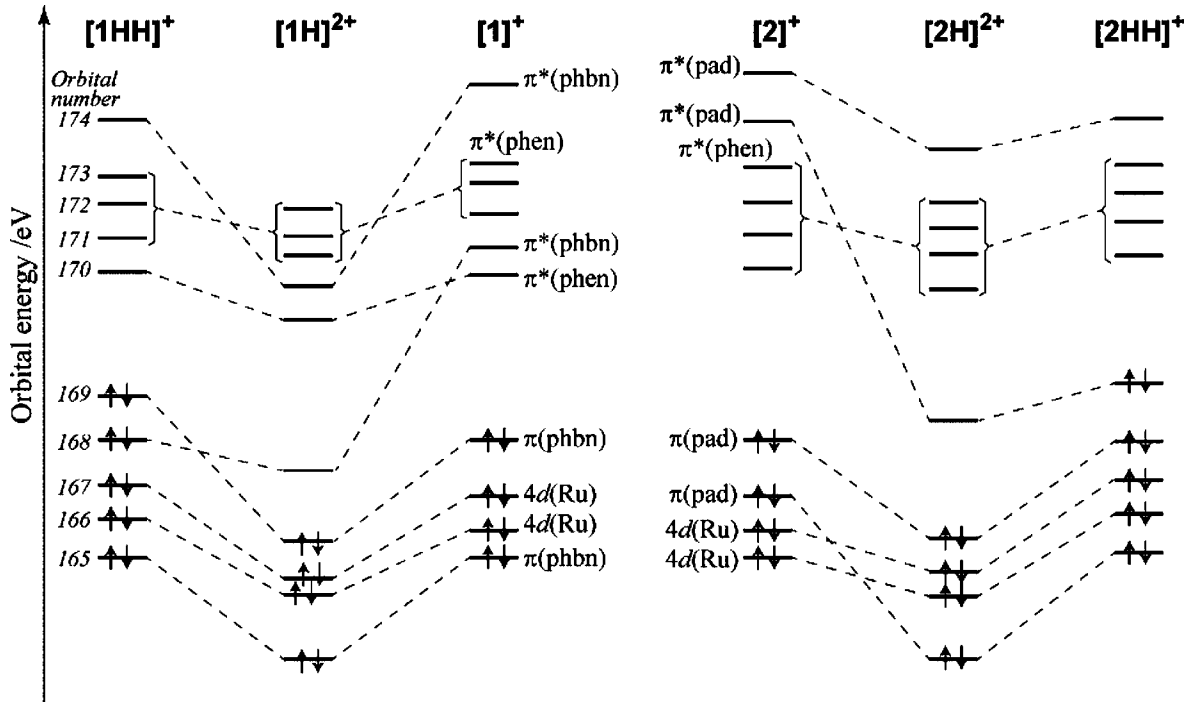

Figure 3. Valence MO diagram and correlation for $[\mathbf{1}]^+$ to $[\mathbf{1HH}]^+$ and $[\mathbf{2}]^+$ to $[\mathbf{2HH}]^+$.

shown in Figure S23 of the Supporting Information, where the full width at half-maximum (fwhm) for the convolution by Gaussian envelope was set to 30 nm. The agreement between the computational and experimental spectra was not perfect mainly because our computation neglected the environmental effects. While, our computation reasonably reproduced the trends of observed spectra, the following were not reproduced: the shoulder around 740 nm for $[\mathbf{1H}]^{2+}$ that was not observed for $[\mathbf{1}]^+$ and $[\mathbf{1HH}]^+$ and a peak at 640 nm for $[\mathbf{2H}]^{2+}$ that was not observed for $[\mathbf{2}]^+$ and $[\mathbf{2HH}]^+$. This indicates our computation can describe the valence electronic structure with reasonable accuracy. Therefore, we can discuss the difference of spectra among these complexes on the basis of the MOs.

The main peak of $[\mathbf{1}]^+$ observed around 540 nm can be assigned to the 3^1A state calculated at 542 nm, whose main transition is the HOMO (highest occupied MO) to LUMO (lowest unoccupied MO)+1; the character of the transition is $\pi(\mathbf{phbn}) \rightarrow \pi^*(\mathbf{phbn})$ and also $4d(\mathrm{Ru}) \rightarrow \pi^*(\mathbf{phbn})$. The low-intensity states were calculated in lower energy rather than the main peak. Their main transitions are the HOMO to LUMO and the HOMO to LUMO+3; the character of the transitions is $\pi(\mathbf{phbn}) \rightarrow \pi^*(\mathrm{phen})$. That is a perpendicular transition like $n \rightarrow \pi^*$; therefore, such transitions are approximately optically forbidden. For $[\mathbf{1H}]^{2+}$, the observed peak around 740 nm may be assigned to the 1^1A and 3^1A states calculated at 1054 and 738 nm, respectively. The excitation energy of the 1^1A state may be underestimated around 0.4 eV. The lowest 1^1A state is the HOMO to LUMO transition. The character of the transition is $\pi(\mathbf{phbnH}) \rightarrow \pi^*(\mathbf{phbnH})$ and also $4d(\mathrm{Ru}) \rightarrow \pi^*(\mathbf{phbnH})$; that is similar to the main peak of $[\mathbf{1}]^+$. The main peak of $[\mathbf{1HH}]^+$ observed around 550 nm can be assigned to the 7^1A and 8^1A states calculated at 502 and 485 nm, respectively. The character of the transitions is $\pi(\mathbf{phbnHH}) \rightarrow \pi^*(\mathrm{phen})$ and $4d(\mathrm{Ru}) \rightarrow \pi^*(\mathrm{phen})$. Because **phbnHH** has a nonplanar structure, such transitions have a larger intensity for $[\mathbf{1HH}]^+$ than the corresponding transitions of $[\mathbf{1}]^+$ and $[\mathbf{1H}]^{2+}$.

For $[\mathbf{2}]^+$, the observed peak around 525 nm can be assigned to the 7^1A state that has the character of metal to ligands (phen) CT excitation. The lowest HOMO−LUMO excitation, the 1^1A state, has the character of $\pi(\mathbf{pad}) \rightarrow \pi^*(\mathrm{phen})$ excitation; however, the intensity is very low. For $[\mathbf{2H}]^{2+}$, the observed peak around 640 nm may be assigned to the 1^1A and 2^1A states calculated at 565 and 535 nm, respectively. The excitation energy of these states may be overestimated 0.2−0.4 eV. Their main transitions are the HOMO to LUMO and the HOMO−1 to LUMO. They have the character of metal to ligands (phen and **padH**) CT and also $\pi(\mathbf{padH}) \rightarrow \pi^*(\mathbf{padH})$ excitations. For $[\mathbf{2HH}]^{2+}$, the observed peak around 525 nm can be assigned to the 11^1A state calculated at 477 nm. The character is metal to ligand (phen) CT; it also participates with a component of $\pi(\mathrm{phen}) \rightarrow \pi^*(\mathrm{phen})$ excitation.

Variation of the character of low-lying electronic excited states among these six complexes can be explained by the energy diagram of valence orbitals, which is shown in Figure 3. Protonation on **phbn** ligand stabilizes the valence orbital energies of $[\mathbf{1H}]^{2+}$ in comparison with those of $[\mathbf{1}]^+$, in particular $\pi^*(\mathbf{phbnH})$ orbitals. Consequently, the character of the LUMO changes between $[\mathbf{1}]^+$ and $[\mathbf{1H}]^{2+}$. The HOMO−LUMO energy gap of $[\mathbf{1H}]^{2+}$ decreases. Thus, excited states with relatively high intensity were calculated and observed for $[\mathbf{1H}]^{2+}$, which were not obtained for $[\mathbf{1}]^+$. In $[\mathbf{1HH}]^{2+}$, the orbital that corresponds to $\pi^*(\mathbf{phbnHH})$ is occupied by electrons. The characters of the HOMO and LUMO of $[\mathbf{1HH}]^{2+}$ are, respectively, $\pi(\mathbf{phbnHH})$ and $\pi^*(\mathrm{phen})$. Those are similar to $[\mathbf{1}]^+$; therefore, the states lower than 700 nm obtained for $[\mathbf{1H}]^{2+}$ disappeared in $[\mathbf{1HH}]^+$. We can see similar findings for the complexes $[\mathbf{2}]^+$, $[\mathbf{2H}]^{2+}$, and $[\mathbf{2HH}]^+$.

Upon protonation, the $\pi^*(\mathbf{padH})$ is more stabilized as compared to the $\pi^*(\mathbf{pad})$ in $[\mathbf{2}]^+$. The relative energy levels of $\pi^*(\mathbf{pad})$ in $[\mathbf{2}]^+$ are higher than those of $\pi^*(\mathbf{phbn})$ in $[\mathbf{1}]^+$. It was also observed in the cyclic voltammogram (vide infra) that the redox couple of ligand **phbn** in $[\mathbf{2}]^+$ appears at ∼300 mV

dx.doi.org/10.1021/ic300449q | Inorg. Chem. 2012, 51, 8091−8102

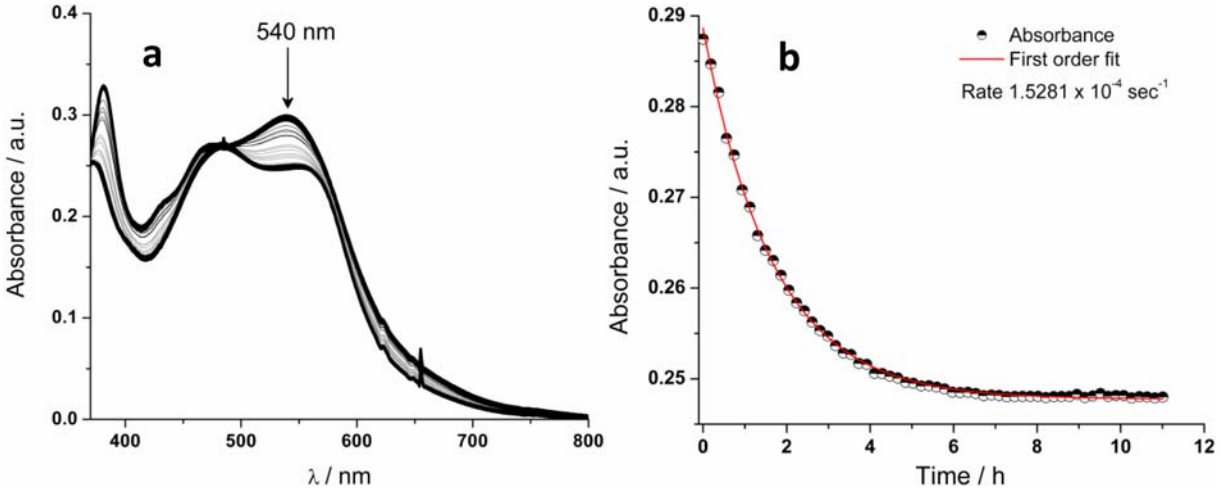

Figure 4. Change in UV–vis spectra of photoinduced reduction of $[\mathbf{1}]PF_6$ in 0.025 mM: (a) CH_3CN/TEA 4:1 v/v upon irradiation with $h\nu \geq 420$ nm and (b) the absorbance vs time profile at 550 nm.

more positive than the **pad**-based redox couple in $[\mathbf{1}]^+$. The HOMO–LUMO energy gap of $[\mathbf{2H}]^{2+}$ is larger than that of $[\mathbf{1H}]^{2+}$, after the stabilization of π^*(**padH**) by protonation. Thus, the lowest excited states of $[\mathbf{2H}]^{2+}$ have higher energies than the corresponding states of $[\mathbf{1H}]^{2+}$. This phenomenon becomes the key factor leading to exhibit an *r*NHC type behavior in $[\mathbf{2H}]^{2+}$.

Photochemical Reduction. The continuous photolysis at ($\lambda \geq 420$ nm) of a 0.025 mM solution of $[\mathbf{1}]PF_6$ in CH_3CN/Et_3N causes a decrease in the absorption bands of $[\mathbf{1}]^+$ at 540 nm and the appearance of a new species at 485 nm (Figure 4a) with a gradual change in color of $[\mathbf{1}]PF_6$ from purple to pink. The ^1H NMR spectra of the product is consistent with the formation of $[\mathbf{1HH}]^+$ by the reaction of two protons and two photoproduced electrons (Yield 67%). The high-resolution electrospray ionization (HR-ESI) mass spectrum of the final solution displayed a parent peak at m/z 719.17, found 719.15 (Calculated with z = 1). We have demonstrated earlier that during photochemical reduction of $[Ru(bpy)_2(\mathbf{pbn})]^{2+}$, photochemically generated $[Ru(bpy)_2(\mathbf{pbn}^{-\bullet})]^+$ undergoes protonation, and the resultant $[Ru(bpy)_2(\mathbf{pbnH}^{\bullet})]^{2+}$ forms an intermediate $\pi\cdots\pi$ dimer $\{[Ru(bpy)_2(\mathbf{pbnH}^{\bullet})]^{2+}\}_2$. The subsequent proton-coupled electron transfer between the two $[Ru(bpy)_2(\mathbf{pbnH}^{\bullet})]^{2+}$ moieties in the dimer originates the disproportionation reaction to produce $[Ru(bpy)_2(\mathbf{pbnHH})]^{2+}$ and $[Ru(bpy)_2(\mathbf{pbn})]^{2+}$. In the present study, we could not observe any intermediate species in the absorption spectra during the photo irradiation like the photochemical reduction of $[Ru(bpy)_2(\mathbf{phbn})]^+$. In this case, the one electron reduced species might be an unstable species. Upon the initial reduction, the radical ligand may be generated (Scheme 6), protonates (Step 1), and then disproportionates ($K_{dis} = 7.5 \times 10^{-10}$; K_{dis} is the disproportionation constant) through electron and proton transfer to afford $[\mathbf{1HH}]^+$ and $[\mathbf{1}]^+$ (Step 2). The rate of conversion of $[\mathbf{1}]^+$ to $[\mathbf{1HH}]^+$ is first order in nature with the rate constant $k = 1.53 \times 10^{-4}$ s^{-1} (Figure 4b). In $[\mathbf{1}]^+$, the (0–0) transition energy is calculated to be +1.61 eV in CH_3CN at 298 K on the basis of the emission maximum 770 nm. The excited state redox potential for the $(Ru^{II}*/Ru^{I})$ couple is correlated with $E_{1/2}(\mathbf{phbn}^{-\bullet}/\mathbf{phbn})$ and $E_{em}(0-0)$ eq 1 and determined to be +0.95 V vs SCE. The redox potential of the $(Ru^{II}*/Ru^{I})$ couple located at a more positive potential than the oxidation potential of sacrificial agent TEA, indicating that electron transfer from TEA to the ruthenium center is highly possible. At 298 K, the (0–0) transition energy of $[\mathbf{2}]^+$ in CH_3CN is +1.70 eV on the basis of the emission maximum 730 nm. The excited state redox potential for the $(Ru^{II}*/Ru^{I})$ is +0.75 V vs SCE, which is almost in the range of oxidation potential of TEA. Therefore, the electron transfer from TEA to the ruthenium center of $[\mathbf{2}]^+$ is highly difficult.

Scheme 6. Mechanistic Approach for the Photochemical Reduction of $[\mathbf{1}]PF_6$

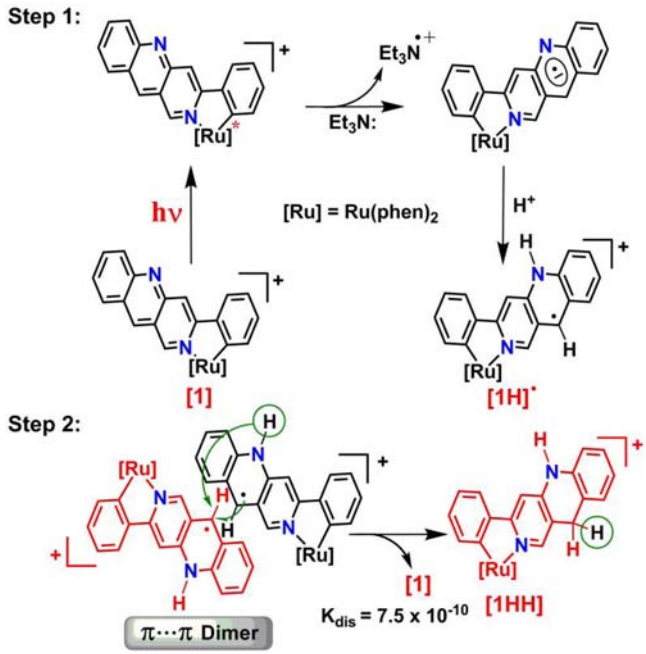

$$E(Ru^{II}*/Ru^{I}) = E_{1/2}(\mathbf{phbn}^{-\bullet}/\mathbf{phbn}) + E_{em}(0-0) \quad (1)$$

Cyclic Voltammetry. The electrochemical data of the complexes are tabulated in Table 3. The cyclic voltammogram of $[\mathbf{1}]PF_6$ in dry CH_3CN exhibits the reversible (Ru^{II}/Ru^{III}) redox couple at $E_{1/2}$ = +0.75 V(vs SCE). One reversible cathodic wave at −0.96 V was observed due to **phbn**/**phbn**$^{-\bullet}$ along with two reversible (phen, phen/phen$^{-\bullet}$, phen) and (phen$^{-\bullet}$, phen/phen$^{-\bullet}$, phen$^{-\bullet}$) redox couples at $E_{1/2}$ = −1.50 V and −1.75 V, respectively (Figure 5a). In complex $[\mathbf{1H}](PF_6)_2$ cathodic peak

dx.doi.org/10.1021/ic300449q | Inorg. Chem. 2012, 51, 8091–8102

Table 3. Electrochemical Data of the Complexes

complexes	$E_{1/2}$ **1**	$E_{1/2}$ **2**	$E_{1/2}$ **3**	$E_{1/2}$ **4**	$E_{1/2}$ **5**	reference
[Ru(**phbn**)(phen)$_2$]$^+$	−1.75 V	−1.50 V	−0.96 V	+0.75 V		this work
[Ru(**phbnH**)(phen)$_2$]$^{2+}$	−1.95 V	−1.55 V	−0.50 V	+0.92 V		this work
[Ru(**phbnHH**)(phen)$_2$]$^+$	−1.20 V	−0.88 V	+1.20 V	+1.45 V[a]		this work
[Ru(**phbn**)(bpy)$_2$]$^+$	−2.02 V	−1.72 V	−0.92 V	+0.51 V		5a
[Ru(**phbnH**)(bpy)$_2$]$^{2+}$	−1.90 V	−1.48 V	−0.84 V	+0.72 V		this work
[Ru(**phbnHH**)(bpy)$_2$]$^+$	−1.92 V	−1.67 V	+0.35 V	+0.55 V	+1.15 V[a]	5a
[Ru(**pad**)(phen)$_2$]$^+$	−1.68 V	−1.35 V	−1.25 V	+0.85 V	+1.12 V	this work
[Ru(**padH**)(phen)$_2$]$^{2+}$	−2.10 V	−1.70 V	−1.0 V	+0.55 V		this work
[Ru(**padHH**)(phen)$_2$]$^+$	−1.15 V	−0.85 V	+1.15 V[a]	+1.50 V		this work
[Ru(**pad**)(bpy)$_2$]$^+$	−1.92 V	−1.64 V	−1.61 V	+0.52 V	+0.78 V	5b
[Ru(**padH**)(bpy)$_2$]$^{2+}$	−2.08 V	−1.68 V	−1.20 V	+0.55 V		this work
[Ru(**padHH**)(bpy)$_2$]$^+$	−1.85 V	−1.61 V	+0.45 V[a]	+0.90 V		5b

[a]These are irreversible anodic oxidation waves of the NADH form.

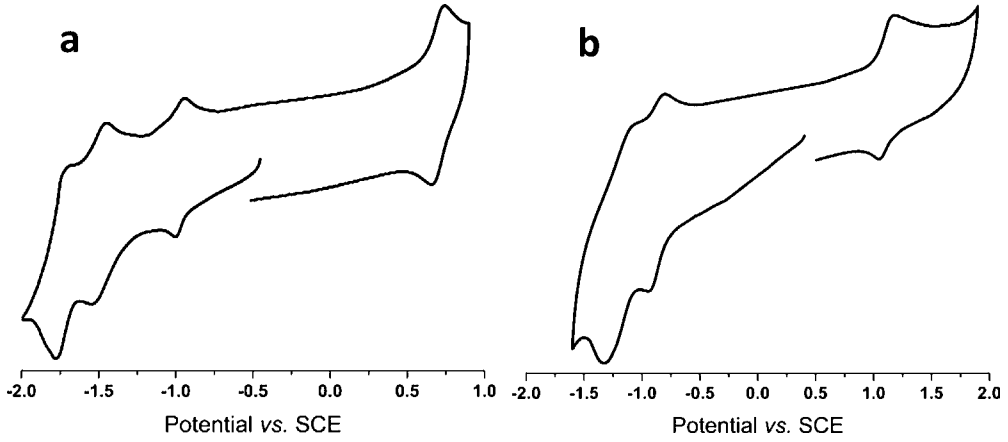

Figure 5. Cyclic voltammogram of 0.1 mM complex solution of (a) [**1**]$^+$ and (b) [**1HH**]$^+$ in CH_3CN containing 0.1 M Bu_4NPF_6 as a supporting electrolyte under dry conditions.

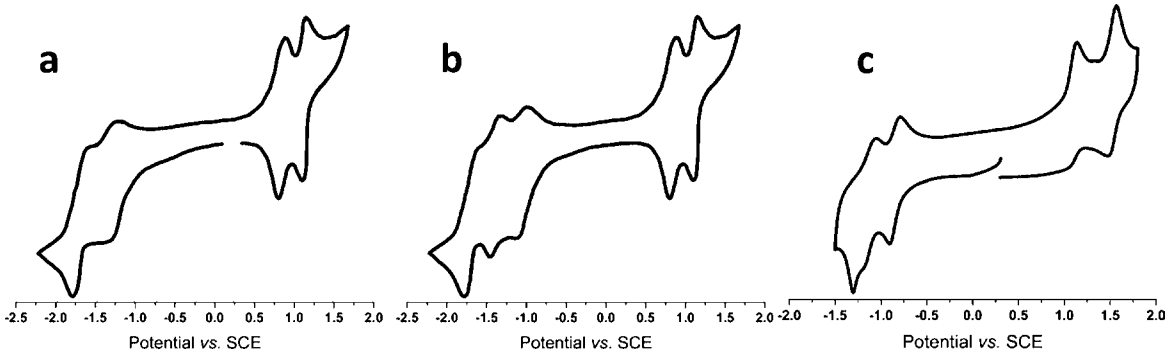

Figure 6. Cyclic voltammogram of 0.1 mM complex solution of (a) [**2**]$^+$ (under dry conditions), (b) with the addition of 10 equiv. of water to [**2**]$^+$, and (c) [**2HH**]$^+$ in CH_3CN containing 0.1 M Bu_4NPF_6 as a supporting electrolyte.

at −0.96 V underwent an anodic shift to −0.50 V. Consumption of 2F/mol of electrons in the exhaustive controlled potential electrolysis of 1 mM [**1**]PF_6 solution in CH_3CN/H_2O (9:1 v/v) containing Bu_4NPF_6 as a supporting electrolyte (0.1 M) at −1.15 V (vs SCE) clarified the irreversible redox reaction as proton coupled two-electron reduction of **phbn** affording **phbnHH**. In the case of [**1HH**]PF_6, the two redox couples at −0.88 and −1.20 V are, respectively, due to the reduction of (phen, phen/phen$^{-\bullet}$, phen) and (phen$^{-\bullet}$, phen/phen$^{-\bullet}$, phen$^{-\bullet}$) (Figure 5b). The reversible redox couple for (Ru^{II}/Ru^{III}) was observed at +1.20 V, and a shoulder merged at +1.45 V was assigned to an irreversible **phbnHH** based oxidation.

The cyclic voltammogram of [**2**]PF_6 in dry CH_3CN exhibits two reversible (Ru^{II}/ Ru^{III}) and (Ru^{III}/ Ru^{IV}) redox couples at $E_{1/2}$ = +0.85 V and +1.12 V (vs SCE), respectively (Figure 6a). A broad cathodic wave appears at −1.25 V as a shoulder of one of the two reversible (phen, phen/phen$^{-\bullet}$, phen) and (phen$^{-\bullet}$, phen/phen$^{-\bullet}$, phen$^{-\bullet}$) redox couples at $E_{1/2}$ = −1.35 V and −1.68 V, respectively. An addition of 10 equivalent of water to the solution shifted the cathodic peak at −1.25 V to −1.05 V (Figure 6b). In complex [**2H**]$(PF_6)_2$ cathodic peak appeared at −1.0 V along with two reversible (phen, phen/phen$^{-\bullet}$, phen) and (phen$^{-\bullet}$, phen/phen$^{-\bullet}$, phen$^{-\bullet}$) redox couples at $E_{1/2}$ = −1.70 V and −2.10 V, respectively. Consumption of 2F/mol of

dx.doi.org/10.1021/ic300449q | Inorg. Chem. 2012, 51, 8091−8102

Scheme 7. Acid Base Equilibrium in Complexes $[1]^+$ and $[2]^+$

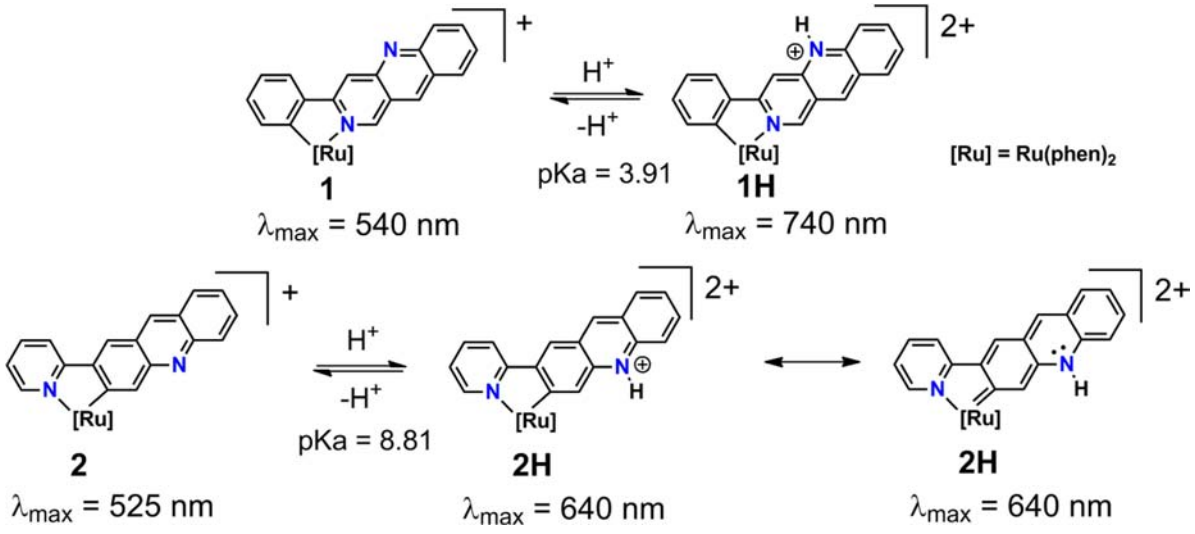

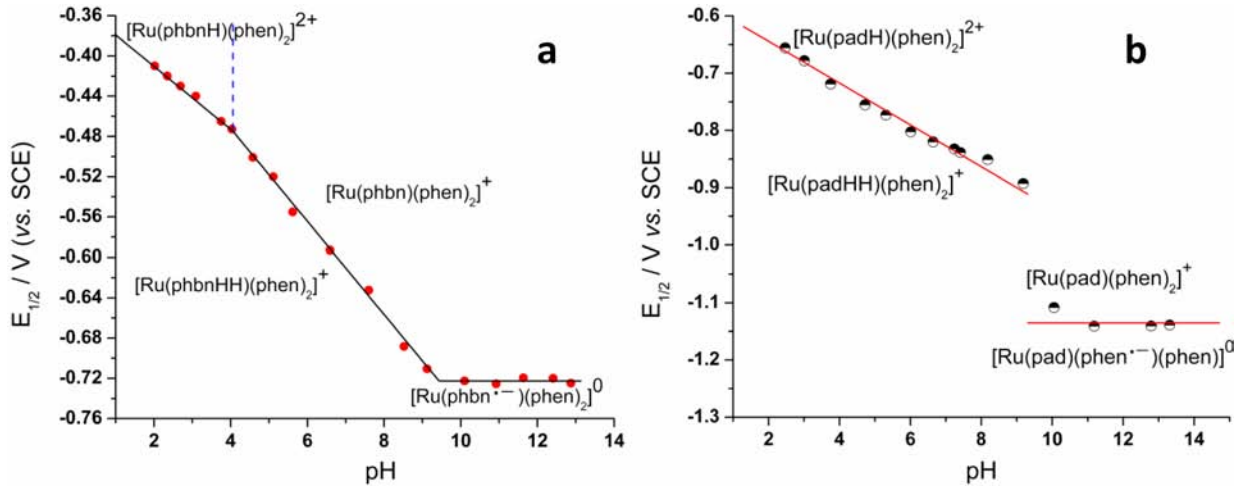

Figure 7. (a) Pourbaix plot of $[1]^+$ and (b) $[2]^+$ using phosphate buffer in aqueous media.

electrons in the exhaustive electrolysis of the resultant solution at −1.20 V (vs SCE) clarified the irreversible redox reaction as proton coupled two-electron reduction of **pad** affording **padHH**. In case of [**2HH**]PF_6, the two redox couples at −0.85 and −1.15 V were, respectively, due to the reduction of (phen, phen/phen$^{-\bullet}$, phen) and (phen$^{-\bullet}$, phen/phen$^{-\bullet}$, phen$^{-\bullet}$) (Figure 6c). An irreversible oxidation wave was observed at the anodic end at +1.15 V, assigned to **padHH**-based oxidation along with the reversible redox couple for (Ru^{II}/Ru^{III}) at +1.50 V.

Acid Base Equilibria and Aqueous Electrochemistry. The pH titration UV−vis spectra of complexes [**1**]PF_6 and [**2**]PF_6 were recorded in aqueous solution containing phosphate buffer, and their analyses are outlined in Scheme 7. In complex $[\mathbf{1H}]^{2+}$, the λ_{max} at 740 nm decreases with an increase in pH, and a new peak at 540 nm emerges. After pH 5.5, there is no change in spectral change observed during pH titration. In the case of complex $[\mathbf{2H}]^{2+}$ with increasing pH, the λ_{max} at 640 nm decreases, and a new peak appeared at 525 nm. In complex $[\mathbf{2H}]^{2+}$, the λ_{max} at 525 nm remains constant beyond pH > 10.5. The pK_a values of $[\mathbf{1H}]^{2+}$ and $[\mathbf{2H}]^{2+}$ were determined to be 3.91 and 8.81, respectively (Figure S20−21, Supporting Information).

In complex $[\mathbf{1}]^+$, within the pH range 2.0−4.0 (Figure 7a), the initial reduction process is −30 mV per pH unit indicating a $2e^-/1H^+$ process of $[Ru^{II}(\mathbf{phbnH})(phen)_2]^{2+}/[Ru^{II}(\mathbf{phbnHH})(phen)_2]^+$. But in between pH 4.0−9.5, the slope is −60 mV per pH unit, signifying a $2e^-/2H^+$ process of $[Ru^{II}(\mathbf{phbn})(phen)_2]^+/[Ru^{II}(\mathbf{phbnHH})(phen)_2]^+$. Beyond pH 9.5, the reduction process is independent of pH and is a $1e^-$ reduction of $[Ru^{II}(\mathbf{phbn})(phen)_2]^+/[Ru^{II}(\mathbf{phbn^{-\bullet}})(phen)_2]^0$. Within the pH range 2.5−9.0, the initial reduction process in the case of $[\mathbf{2}]^+$ is −30 mV per pH unit, indicating a $2e^-/1H^+$ process of $[Ru(\mathbf{padH})(phen)_2]^{2+}/[Ru(\mathbf{padHH})(phen)_2]^+$ (Figure 7b). Beyond pH 9, the cyclic voltammogram of $[\mathbf{2}]^+$ displays the pH independent $1e^-$ reduction of $[Ru(\mathbf{pad})(phen)_2]^+/[Ru(\mathbf{pad})(phen^{-\bullet})(phen)]^0$.

Electrochemical Reduction and Spectrochemistry. Under controlled potential electrolysis, the electrolytic reduction 0.05 mM of [**1**]PF_6 containing Bu_4NPF_6 as a supporting electrolyte (0.1 M) in an acetonitrile/H_2O (9:1 v/v) mixture was carried out at −1.15 V (vs SCE) in an argon atmosphere at 25 °C. An electrolysis UV cell of path length 0.05 cm consisting of three components, the working (platinum mesh) and the counter (platinum plate) electrodes, was used. The reference electrode ($Ag/AgNO_3$, +0.30 V vs SCE) was separated from the working compartment by a Vycor glass. In this case, the peak at 540 nm decreases with an increase

dx.doi.org/10.1021/ic300449q | Inorg. Chem. 2012, 51, 8091−8102

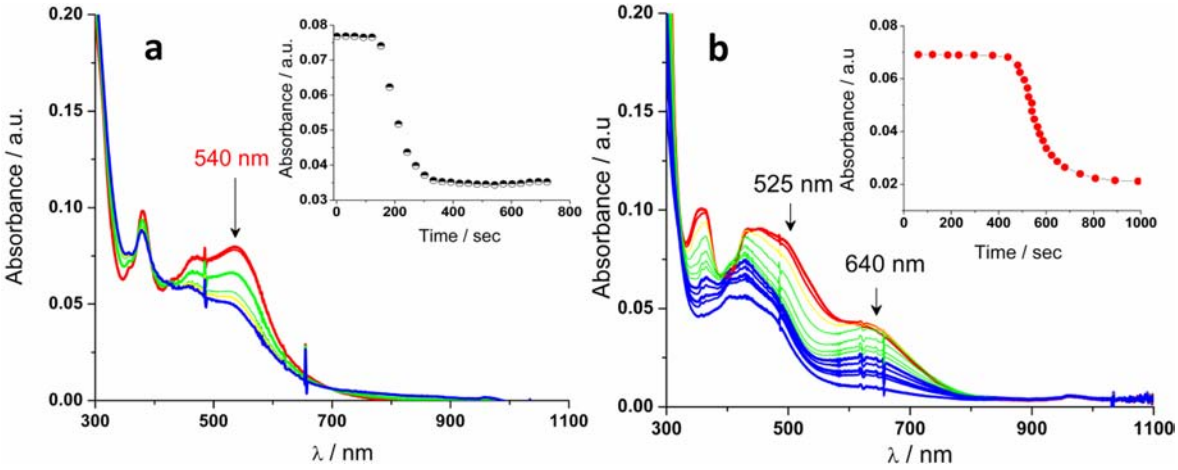

Figure 8. Change in UV–vis spectra (cell path length, 0.05 cm) during electrochemical reduction of (a) $[\mathbf{1}]PF_6$ and (b) $[\mathbf{2}]PF_6$ in CH_3CN:H_2O (9:1) containing Bu_4NPF_6 as a supporting electrolyte (0.1 M) with a complex concentration of 0.05 mM. Inset is the absorbance vs time profile at 540 and 525 nm for $[\mathbf{1}]PF_6$ and $[\mathbf{2}]PF_6$, respectively.

in intensity of the band at 450 nm, which is similar to the UV–vis spectra of $[\mathbf{1HH}]^+$ after the completion of the reaction (Figure 8a). The final product was isolated and confirmed from the ^{1}H NMR spectra. In a similar procedure, the electrolytic reduction was carried out for complex $[\mathbf{2}](PF_6)$. The peaks at 640 and 525 nm decreases with emerging peak intensity at 425 nm (Figure 8b). The final product was isolated and analyzed by proton ^{1}H NMR spectra, confirming the formation of $[\mathbf{2HH}](PF_6)$.

Dynamic Equilibrium in $[\mathbf{2H}]^{2+}$. In the case of $[\mathbf{2H}](PF_6)_2$, the π-accepting ability of the coordinated carbon center increases due to protonation with a decrease in energy of the π^* orbital in **pad** after protonation as compared to the non-protonated form $[\mathbf{2}](PF_6)$. The ^{13}C NMR of the coordinated carbon in complex $[\mathbf{2H}](PF_6)_2$ appears at 254.41 ppm. In our previous report, it has been reported that in the case of $[Ru(\mathbf{padH})(bpy)_2](PF_6)_2$ the ^{13}C NMR peak appears at 228.87 ppm. It is a significant feature of remote N-heterocyclic carbene (*r*NHC) type behavior. Upon protonation, the Ru–C bond exists in a tautomeric equilibrium with Ru=C coordination (eq 2). This is in agreement with the theorical results (vide

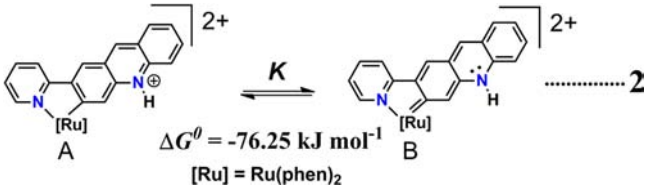

supra) for the shorter Ru–C bond (2.016 Å; in the case of $[Ru(\mathbf{padH})(bpy)_2)]^{2+}$, it is 2.011 Å from the single crystal X-ray structure[5b]) in $[\mathbf{2H}]^{2+}$ than in $[\mathbf{2}]^+$. The electronic structure of the protonated complex may be an intermediate canonical form of the contributing structures Ru^{II}–C and Ru^{IV}=C. The ^{13}C NMR signal of the remote N-heterocyclic carbene (*r*NHC) is reported in the range of 170–200 ppm.[6] In the case of $[\mathbf{1H}](PF_6)_2$, there is no such peak at the downfield region.

The dynamic equilibrium between the Ru–C bond and Ru=C coordination was also supported by the temperature dependent ^{1}H NMR of $[\mathbf{2H}](PF_6)_2$ in CD_3CN. The signal of the adjacent proton (H_a) to the coordinated carbon center and the proton (H_b) (Figure 9) undergo a shielding effect,

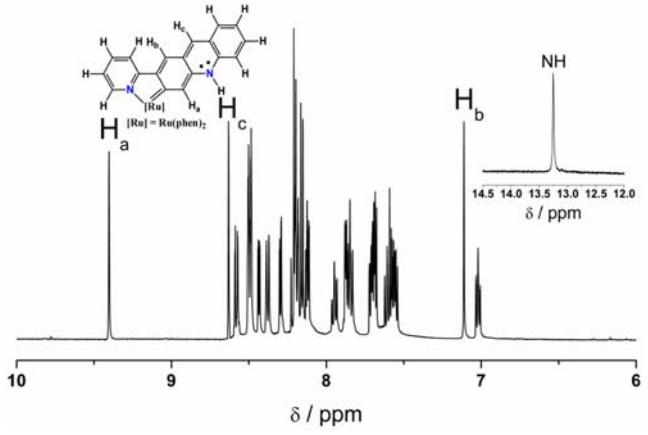

Figure 9. ^{1}H NMR of complex $[\mathbf{2H}]^+$ in CD_3CN at 20 °C.

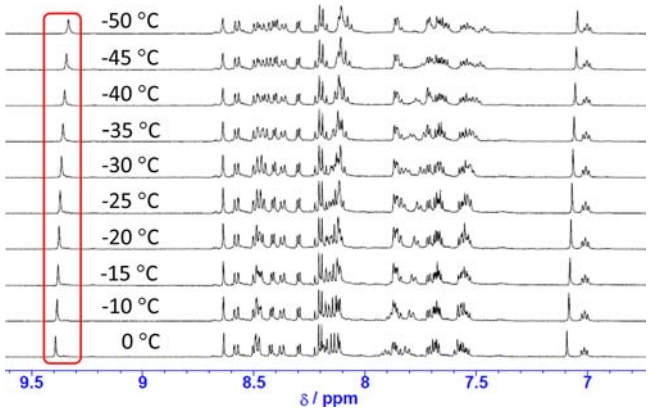

Figure 10. Change in ^{1}H NMR of complex $[\mathbf{2H}]^+$ in CD_3CN with lowering of temperature.

signifying the increase in Ru=C type contribution with the lowering of temperature (Figure 10). But the shielding effect of H_a is higher than that of H_b. The equilibrium constant of eq 2 is defined as $K = (1 - x)/x$; where $x = [\delta_{obs} - \delta(B)]/[\delta(A) - \delta(B)]$ ($\delta(A)$ and $\delta(B)$ are the chemical shifts of A and B species. The most reasonable linear plot of ln K vs T^{-1} (Figure S22,

dx.doi.org/10.1021/ic300449q | Inorg. Chem. 2012, 51, 8091–8102

Supporting Information) was generated using computer simulation with $\delta(A) = 9.403$ and $\delta(B) = 9.334$ for the adjacent proton H_a to the coordinated carbon center at higher temperature and lower temperature, respectively. The standard enthalpy change ΔH^0, entropy change ΔS^0, and free energy ΔG^0 change were determined to be −36.39 kJ mol^{-1}, −0.146/kJ K^{-1} mol^{-1}, and −76.25 kJ mol^{-1}, respectively, from the Vukancic−Vukovic equation.

EXPERIMENTAL SECTION

Instrumentation and Materials. All the manipulations were carried out using standard Schlenk techniques under nitrogen atmosphere. Solvents like dichloromethane, acetonitrile, methanol, 2-methoxyethanol, and hexane were dried, degassed, and stored under nitrogen atmosphere prior to use. NMR spectra were recorded on a JEOL JNM-A500 spectrometer (500 MHz for ^1H and 125 MHz for ^{13}C) at room temperature. High-resolution ESI mass spectra were recorded on a Waters Micromass LCT. The UV−vis-NIR spectra were recorded on a Shimadzu UVPC-3100 PC UV−vis-NIR scanning spectrophotometer or on an Agilent 8543A diode-array spectrophotometer. Emission spectra were recorded on a JASCO FP-6600 spectrofluorometer. Both Cyclic voltammetry and controlled-potential electrolysis were carried out under argon atmosphere. Cyclic voltammetry was carried out using an ALS/Chi model 660A electrochemical analyzer under argon atmosphere at 25 °C at a scan rate of 50 mV in acetonitrile containing Bu_4NPF_6 as a supporting electrolyte (0.1 M) with a complex concentration of 1.0 mM. The working, auxiliary and reference electrodes were AS glassy carbon electrode, platinum wire, and $Ag/AgNO_3$ (0.01 M, BAS RE-5, +0.30 V vs SCE), respectively.

Computational Details. The molecular equilibrium geometries of $[\mathbf{1}]^+$, $[\mathbf{1H}]^{2+}$, $[\mathbf{1HH}]^+$, $[\mathbf{2}]^+$, $[\mathbf{2H}]^{2+}$, and $[\mathbf{2HH}]^+$ were optimized in their singlet ground state by density functional theory (DFT) using B3LYP functional with a 6-31G** basis set for H, C, and N atoms and LANL2DZ pseudo-potential for Ru. The electronic excitation energies and oscillator strengths were calculated using time-dependent (TD) DFT with PBE0 functional (PBE1PBE in GAUSSIAN keyword) and the above-mentioned basis sets. Any environmental effects such as solvent and counterion were not considered. All computations were performed using GAUSSIAN 09 program.

Synthesis. *Synthesis of ([1]PF_6).* To a solution of [Ru(**phbn**)-$(CH_3CN)_4$]PF_6 (0.400 g, 0.60 mmol) in 50 mL of 2-methoxyethanol, 1,10-phenanthroline monohydrate (0.240 g, 1.2 mmol) and a saturated aqueous solution of $NaPF_6$ (0.100 g, 0.6 mmol) were added. The above reaction mixture was refluxed at 80 °C for 24 h. The crude product was evaporated to dryness and purified by column chromatography on neutral alumina using CH_2Cl_2/Acetone by 99:1 (v/v) ratio to give $[\mathbf{1}]PF_6$ of (0.380 g, 0.43 mmol, Yield: 72%). HRMS (ESI): Calc. for $C_{42}H_{27}N_6Ru$ $[\mathbf{1}]^+$ m/z 717.13, found 713.17. Calc. for $C_{42}H_{27}F_6N_6PRu$: %C 58.54, %H 3.16, %N 9.75; found %C 58.61, %H 3.21, %N 9.79. The ^1H NMR (500 MHz, CD_3CN) δ, ppm (J, Hz): 6.28 (1H, d, 6.10), 6.72(1H, t, 7.93), 6.91 (1H, t, 7.63), 7.43 (1H, t, 6.71), 7.51−7.55 (1H, m), 7.60−7.64 (1H, m), 7.67−7.72 (2H, m), 7.83−7.87 (2H, m), 7.92−7.95 (2H, m), 8.02−8.14 (3H, m), 8.19 (1H, d, 8.54), 8.24 (1H, s), 8.34(2H, t, 8.53), 8.40 (2H, t, 8.53), 8.51(1H, s), 8.54−8.59(2H, m), 8.63 (1H, d, 6.71), 8.72 (1H, s), 9.05 (1H, d, 6.10). The 125.65 MHz ^{13}C NMR (δ, (J, Hz), CD_3CN): 163.30, 158.41, 155.17, 153.80, 152.87, 151.55, 151.29, 150.95, 150.85, 149.79, 148.60, 145.91, 137.35, 136.36, 136.28, 135.33, 133.86, 133.79, 133.57, 131.83, 131.80, 131.53, 131.21, 131.09, 130.12, 129.74, 128.92, 128.87, 128.59, 128.43, 128.36, 127.59, 127.37, 127.28, 126.69, 125.98, 125.74, 124.59, 124.25, 122.50, 122.24, 114.23.

Synthesis of [1H](PF_6)$_2$. A solution of $[\mathbf{1}]PF_6$ (0.100 g, 0.12 mmol) in a round-bottomed flask containing 20 mL of CH_2Cl_2 was dropwise added with 0.05 N HPF_6 solution until the color of the solution turned to orange. The stirring was continued for 20 min. The resulting solution was evaporated to a minimum of CH_2Cl_2 solution, and n-hexane was added. A brown colored precipitate was collected under centrifugation followed by washing with ice-cold methanol gives pure $[\mathbf{1H}](PF_6)_2$ (0.100 g (0.100 mmol), Yield: 83%). HRMS (ESI): Calc. for $C_{42}H_{28}N_6Ru$ $[\mathbf{1H}]^{2+}$ m/z 359.07, found 359.11. Calc. for $C_{42}H_{28}F_{12}N_6P_2Ru$: %C 50.06, %H 2.80, %N 8.34; found %C 50.11, %H 2.84, %N 8.38. The ^1H NMR (500 MHz, CD_3CN) δ, ppm (J, Hz): 7.46 (1H, t, 6.71), 7.57−7.63 (2H, m), 7.66−7.71 (2H,m), 7.74 (1H, t, 7.62), 7.83 (1H, d, 5.49), 8.02(1H, d, 6.71), 8.10−8.17 (6H, m), 8.21 (2H, d, 9.15), 8.25−8.27 (2H, m), 8.36−8.46 (3H, m), 8.58 (2H, t, 8.84), 8.76 (1H, s), 8.95 (2H, d, 9.76), 9.12 (NH, s), 9.12 (1H, d, 6.71). The 125.65 MHz ^{13}C NMR (δ, (J, Hz), CD_3CN): 155.98, 155.34, 154.32, 154.13, 151.58, 151.53, 149.83, 149.11, 148.57, 148.38, 143.44, 143.03, 138.51, 137.92, 137.03, 136.96, 135.87, 135.77, 132.14, 131.90, 131.66, 131.48, 131.16, 129.20, 129.01, 128.95, 128.92, 128.88, 128.76, 128.71, 128.66, 128.58, 128.45, 127.25, 127.11, 127.02, 126.91, 126.44, 126.34, 125.73, 125.68, 123.01.

Synthesis of ([1HH]PF_6). Method 1. A solution of $[\mathbf{1}]PF_6$ (0.100 g, 0.12 mmol) in a two-necked round-bottomed flask containing 20 mL of methanol/H_2O (9:1 v/v) was purged under nitrogen for 30 min at −10 °C. The solid $NaBH_4$ (10 mg, 0.26 mmol) was directly added into the solution and allowed to stir for 1 h. A pink colored precipitate was collected under centrifugation followed by washing with an ice-cold methanol/H_2O (9:1 v/v) mixture gives pure $[\mathbf{1HH}]PF_6$ (0.09 g (0.104 mmol), Yield: 87%). HRMS (ESI): Calc. for $C_{42}H_{29}N_6Ru$ $[\mathbf{1HH}]^+$ m/z 719.15, found 719.17. Calc. for $C_{42}H_{29}F_6N_6PRu$: %C 58.40, %H 3.38, %N 9.73; found %C 58.44, %H 3.43, %N 9.76. The ^1H NMR (500 MHz, CD_3CN) δ, ppm (J, Hz): 3.50 (1H, d, 19.53), 3.72 (1H, d, 19.53), 4.57 (NH, s), 6.23 (1H,d, 7.32), 6.66 (1H, t, 7.32), 6.79−6.84 (3H, m), 6.92(1H, d, 7.35), 7.05 (1H, t, 7.32), 7.37 (1H, t, 7.33), 7.45 (1H, s), 7.59−7.62 (3H, m), 7.67 (1H, d, 7.94), 7.83 (1H, d, 5.49), 8.04−8.10 (4H, m), 8.14 (2H, s), 8.26(1H, d, 8.54), 8.31 (1H, d, 7.94), 8.37 (1H, d, 7.93), 8.42 (1H, d, 5.49), 8.46 (1H, d, 8.50), 8.51 (1H, d, 4.89). The 125.65 MHz ^{13}C NMR (δ, (J, Hz), CD_3CN): 163.75, 155.47, 152.07, 151.53, 150.72, 150.04, 149.47, 149.01, 147.29, 141.12, 140.93, 137.54, 136.45, 135.93, 134.52, 133.21, 132.96, 132.28, 131.77, 131.51, 131.26, 129.64, 128.84, 128.76, 128.71, 128.63, 128.52, 128.43, 128.36, 128.31, 126.51, 126.08, 126.00, 125.92, 125.74, 124.07, 122.79, 122.28, 121.70, 120.40, 115.37, 28.00.

Method 2. Visible light ($\lambda \geq 420$ nm) was irradiated to a solution of $[\mathbf{1}]PF_6$ (0.100 g, 0.12 mmol) in 20 mL of CH_3CN/TEA (4:1 v/v) (TEA = triethylamine) solution over 24 h using a 100 W mercury lamp with a cutoff filter (0.5 M $NaNO_2$ solution). The reaction mixture was evaporated to dryness, dissolved in 1 mL of CH_3CN, and precipitated with the addition of water. The pink colored precipitates were centifuged and washed several times with water to give a pure $[\mathbf{1HH}]PF_6$ (0.07 g (0.08 mmol), Yield: 67%). It was characterized by ESI-MS, UV−vis, and NMR spectroscopic measurements. All the spectral measurements were identical with those of isolated in chemical reduction method using $NaBH_4$ as the reducing agent.

Synthesis of [2]PF_6. To a solution of [Ru(**pad**)$(CH_3CN)_4$]PF_6 (0.300 g, 0.45 mmol) in 30 mL of 2-methoxyethanol 1,10-phenanthroline monohydrate (0.180 g, 0.90 mmol) was added a saturated aqueous solution of $NaPF_6$ (0.075 g, 0.45 mmol). The above reaction mixture was refluxed at 80 °C for overnight. The crude product was a mixture of $[\mathbf{2}]PF_6$ and $[\mathbf{2H}](PF_6)_2$ as inferred from the mass spectrum. Further, it was washed with 1 mL of Et_3N and purified by column chromatography on neutral alumina using CH_2Cl_2/Acetone by 99:1 (v/v) ratio to give $[\mathbf{2}]PF_6$ of (0.300 g, 0.35 mmol, Yield: 78%). HRMS (ESI): Calc. for $C_{42}H_{27}N_6Ru$ $[\mathbf{1}]^+$ m/z 717.13, found 717.28. Calc. for $C_{42}H_{27}F_6N_6PRu$: %C 58.54, %H 3.16, %N 9.75; found %C 58.59, %H 3.23, %N 9.81. The 500 MHz ^1H NMR (δ, (J, Hz), CD_3CN): 6.82 (1H, s), 6.94 (1H, t, 7.32), 7.39 (1H, t, 7.75), 7.46 (1H, t, 6.71), 7.52 (1H, t, 6.71), 7.61 (2H, t, 6.71), 7.66 (2H, m), 7.77 (2H, m), 7.91(1H, d, 4.5), 7.96(1H, d, 8.5), 8.04−8.06(2H, m), 8.14−8.18 (2H, m), 8.20(1H, d, 6.72), 8.33−8.37(4H, m), 8.41(1H, d, 9.15), 8.52(1H, d, 9.25), 8.57(1H, s), 8.58(1H, d, 4.88), 8.84(1H, s). The 125.65 MHz ^{13}C NMR (δ, (J, Hz), CD_3CN): 155.30, 152.66, 152.43, 151.90, 151.70, 151.03, 149.73, 149.57, 149.14, 149.03, 148.71, 147.15, 146.93, 137.11, 137.06, 136.84, 136.66, 136.61, 135.67, 135.55, 134.60, 134.41, 131.82, 131.62, 131.57, 131.28, 131.26, 129.48, 128.80,

dx.doi.org/10.1021/ic300449q | Inorg. Chem. 2012, 51, 8091−8102

128.74, 128.60, 126.69, 126.55, 126.29, 126.24, 126.11, 126.08, 125.78, 125.10, 124.66, 122.36, 121.41.

Synthesis of [2H](PF$_6$)$_2$. A solution of [**2**]PF$_6$ (0.08 g, 0. 09 mmol) in a round-bottomed flask containing 20 mL of CH_2Cl_2 was dropwise added with a 0.05 N HPF_6 solution until the color of the solution turned to orange. The stirring was continued for 20 min. The resulting solution was evaporated to a minimum of CH_2Cl_2 solution and an excess of *n*-hexane was added. A brown colored precipitate was collected under centrifugation followed by washing with ice-cold methanol gives pure [**2H**](PF$_6$)$_2$ (0.07 g (0.07 mmol), Yield: 78%). HRMS (ESI): Calc. for $C_{42}H_{28}N_6Ru$ [**2H**]$^{2+}$ *m*/*z* 359.07, found 359.13. Calc. for $C_{42}H_{28}F_{12}N_6P_2Ru$: %C 50.06, %H 2.80, %N 8.34; found %C 50.09, %H 2.82, %N 8.40. The ^{1}H NMR (500 MHz, CD_3CN) δ, ppm (*J*, Hz): 7.02 (1H, t, 7.32), 7.11 (1H, s), 7.54−7.62 (3H, m), 7.67−7.72 (3H, m), 7.83−7.87 (3H, m), 7.95 (1H, t, 7.93), 8.12 (2H, t, 5.50), 8.15 (2H, d, 6.72), 8.17−8.22 (3H, m), 8.30 (1H, d, 6.71), 8.37 (1H, d, 7.95), 8.43 (1H, d, 6.0), 8.50 (2H, d, 9.65), 8.58 (1H, d, 9.30), 8.63 (1H, s), 9.40 (1H, s), 13.25 (NH, s). The 125.65 MHz ^{13}C NMR (δ, (*J*, Hz), CD_3CN): 254.41, 154.90, 154.06, 152.91, 152.32, 152,23, 150.98, 150.39, 149.17, 146.13, 141.23, 137.86, 137.56, 136.95, 136.48, 135.62, 135.45, 133.72, 131.73, 131.66, 131.16, 130.62, 128.94, 128.87, 128.84, 128.79, 127.08, 126.99, 126.85, 126.47, 126.25, 126.08, 125.74, 124.96, 124.58, 123.37, 122.44, 122.04, 120.03, 119.31, 118.81, 117.88.

Synthesis of [2HH]PF$_6$. A solution of [**2**]PF$_6$ (0.100 g, 0.12 mmol) in a two-necked round-bottomed flask containing 20 mL of methanol/H_2O (9:1 v/v) was purged under nitrogen for 30 min at −10 °C. The solid $NaBH_4$ (10 mg, 0.26 mmol) was directly added into the solution and allowed to stir for 1 h. The resulting mixture was evaporated to a minimum volume of methanol followed by the addition of water. A dark red colored precipitate was collected under centrifugation followed by washing with an ice-cold methanol/H_2O (9:1 v/v) mixture gives pure [**2HH**]PF$_6$ (0.085 g (0.098 mmol), Yield: 82%). HRMS (ESI): Calc. for $C_{42}H_{29}N_6Ru$ [**2HH**]$^+$ *m*/*z* 719.13, found 719.28. Calc. for $C_{42}H_{29}F_6N_6PRu$: %C 58.40, %H 3.38, %N 9.73; found %C 58.45, %H 3.41, %N 9.79. The 500 MHz ^{1}H NMR (δ, (*J*, Hz), CD_3CN): 3.91 (1H, d, 18.92), 3.98 (1H, d, 18.92), 5.60(NH, s), 6.50 (1H, d, 7.93), 6.62(1H, s), 6.65(1H, t, 5.0), 6.72 (1H, t, 7.93), 6.94 (1H, t, 7.5), 7.02 (1H, d, 7.32), 7.42 (2H, t, 6.71), 7.54−7.64 (5H, m), 7.85 (2H, t, 7.01), 8.09−8.14 (5H, m), 8.28(1H, d, 6.10), 8.33(2H, t, 7.93), 8.37 (1H, d, 9.05), 8.46 (1H, d, 9.15), 8.60 (1H, d, 6.71). The 125.65 MHz ^{13}C NMR (δ, (*J*, Hz), CD_3CN): 156.00, 152.51, 152.07, 151.92, 151.63, 151.58, 150.94, 142.11, 141.57, 136.55, 136.27, 135.67, 135.02, 134.53, 134.44, 133.97, 133.62, 131.47, 129.53, 129.49, 128.94, 128.87, 128.77, 128.71, 128.59, 127.89, 126.76, 126.42, 126.28, 126.20, 126.13, 125.71, 125.01, 124.66, 122.82, 121.47, 121.41, 121.14, 120.32, 114.48, 114.20, 31.64.

CONCLUSION

From the comparison of spectroscopic and theoretical data of the prescribed complexes, it is concludeed that the position and bonding behavior of σ-coordinating carbon center in C^N and N^C type cyclometalated ligands leads to a significant variation in their properties. Both complexes [**1**]$^+$ and [**2**]$^+$ undergo chemical and electrochemical reduction to generate their corresponding reduced form [**1HH**]$^+$ and [**2HH**]$^+$, respectively. The redox potential of the (Ru^{II}*/Ru^{I}) couple (+0.95 vs SCE) in [**1**]$^+$ is located at more a positive potential than the oxidation potential of the sacrificial agent TEA; therefore, the electron transfer from TEA to the ruthenium center is highly possible. However, the redox potential of the (Ru^{II}*/Ru^{I}) couple (+0.75 vs SCE) in [**2**]$^+$ is almost equal to the oxidation potential of TEA. Therefore, the photochemical reduction of [**2**]$^+$ in the presence of TEA was not successful. The cyclic voltammogram of [**1**]$^+$ in dry CH_3CN indicates that the reduction of the C^N type ligand **phbn** reduced around ∼300 mV more positive potential compared to the N^C type ligand **pad** in [**2**]$^+$, which was also supported by the theoretical data that the energy level of the π* orbital of **pad** in [**2**]$^+$ is higher than that of the π* orbital of **phbn** in [**1**]$^+$. It has also been noticed that the electrochemical reduction of [**1**]$^+$ is faster than [**2**]$^+$ due to the more positive redox potential of **phbn**. The HOMO−LUMO energy difference in [**2H**]$^{2+}$ is larger than that of [**1H**]$^{2+}$, after the stabilization of π*(**padH**) by protonation. Therefore, the lowest excited states of [**2H**]$^{2+}$ have higher energies compared to the corresponding states of [**1H**]$^{2+}$. Complex [**2H**](PF$_6$)$_2$, the optimized structure, reveals that upon protonation the Ru−C bond distance shortens both in [**1**]$^+$ and [**2**]$^+$. In [**2H**]$^{2+}$, the Ru−C exists in a proton-induced dynamic equilibrium with Ru═C and behaves as a remote N-heterocyclic carbene (*r*NHC). It was also clarified from the ^{13}C NMR spectra (appears at 254.41 ppm) of [**2H**](PF$_6$)$_2$ in CD_3CN. The standard free energy change of the tautomeric equilibrium between Ru−C and Ru═C type coordination is −76.25 kJ mol^{-1}. But this type of behavior was not noticed in [**1H**](PF$_6$)$_2$.

ASSOCIATED CONTENT

Supporting Information

Characterization, and DFT calculations (PDF) data are provided. This material is available free of charge via the Internet at http://pubs.acs.org.

AUTHOR INFORMATION

Corresponding Author

*E-mail: ktanaka@ims.ac.jp, koji.tanaka@icems.kyoto-u.ac.jp.

Notes

The authors declare no competing financial interest.

ACKNOWLEDGMENTS

This work is supported by a Grand-in-Aid for Specially Promoted Research (Grant 20002005) from the Ministry of Education, Culture, Sports, Science, and Technology of Japan.

REFERENCES

(1) (a) Photosynthesis. In *McGraw-Hill Encyclopedia of Science and Technology*; McGraw-Hill: New York, 2007; p 472. (b) Hill, R. *Proc. R. Soc. B* **1939**, *127* (847), 192−210. (c) Priestley, J. *Observations on Different Kinds of Air*; Phil. Trans.: London, 1772; Vol. *62*, pp 147−264. (d) Berg, J. M.; Tymoczko, J. L.; Stryer, L. *Biochemistry*, 6 ed.; W.H. Freeman: New York, 2007.

(2) (a) Bassham, J.; Benson, A.; Calvin, M. *J. Biol. Chem.* **1950**, *185* (2), 781−787. (b) Dau, H.; Haumann, M. *Coord. Chem. Rev.* **2008**, *252*, 273−295. (c) Yano, J.; Kern, J.; Sauer, K.; Latimer, M. J.; Pushkar, Y.; Biesiadka, J.; Loll, B.; Saenger, W.; Messinger, J.; Zouni, A.; Yachandra, V. K. *Science* **2006**, *314*, 821−825. (d) Eisner, U.; Kuthan, J. *Chem. Rev.* **1972**, *72*, 1. (e) Walsh, C. *Acc. Chem. Res.* **1980**, *13*, 148. (f) Stout, D. M.; Meyers, A. I. *Chem. Rev.* **1982**, *82*, 223.

(3) (a) Magnuson, A.; Anderlund, M.; Johansson, O.; Lindblad, P.; Lomoth, R.; Polivka, T.; Ott, S.; Stensjo., K.; Styring, S.; Sundstro.m, V.; Hammarstro.m, L. *Acc. Chem. Res.* **2009**, *42*, 1899−1909. (b) Ghirardi, M. L.; Dubini, A.; Yu, J.; Maness, P. C. *Chem. Soc. Rev.* **2009**, *38*, 52−61. (c) Malki, S.; Saimmaime, I.; Luca, D. G.; Rousset, M.; Dermoun, Z.; Belaich., J. P. *J. Bacteriol.* **1995**, *177*, 2628−2636. (d) Soboh, B.; Linder, D.; Hedderich., R. *Microbiology* **2004**, *150*, 2451−2463. (e) Schut, G. J.; Adams, W. W. *J. Bacteriol.* **2009**, *191*, 4451−4457. (f) Liebgott, P.-P.; De Lacey, A. L.; Burlat, B.; Cournac, L.; Richaud, P.; Brugna, M.; Fernandez, V. M.; Guigliarelli, B.; Rousset, M.; Le.ger, C.; Dementin, S. *J. Am. Chem. Soc.* **2011**, *133*, 986−997. (g) Fukuzumi, S. In *Advances in Electron-Transfer Chemistry*; Mariano, P. S., Ed.; JAI Press, Inc.: Greenwich, CT, 1992; pp 67−175, and references therein. (h) Gębicki, J.; Marcinek, A.; Zielonka, J. *Acc. Chem. Res.* **2004**, *37*, 379.

(4) (a) Cohen, B. W.; Polyansky, D. E.; Achord, P.; Cabelli, D.; Muckerman, J. T.; Tanaka, K.; Thummel, R. P.; Zong, R.; Fujita, E. *Faraday Discuss.* **2012**, *155*, 129−144. (b) Ohtsu, H.; Tanaka, K. *Chem. Commun.* **2012**, *48*, 1796−1798. (c) Fukushima, T.; Wada, T.; Ohtsu, H.; Tanaka, K. *Dalton Trans.* **2010**, *39*, 11526−11534. (d) Cohen, B. W.; Polyansky, D. E.; Zong, R. F.; Zhou, H.; Ouk, T.; Cabelli, D. E.; Thummel, R. P.; Fujita, E. *Inorg. Chem.* **2010**, *49*, 8034−8044. (e) Matsubara, Y.; Koga, K.; Kobayashi, A.; Konno, H.; Sakamoto, K.; Morimoto, T.; Ishitani, O. *J. Am. Chem. Soc.* **2010**, *132*, 10547−10552. (f) Tanaka, K. *Chem. Rec.* **2009**, *9*, 169. (g) Fukushima, T.; Fujita, E.; Muckerman, J. T.; Polyansky, D. E.; Wada, T.; Tanaka, K. *Inorg. Chem.* **2009**, *48*, 11510−11512. (h) Polyansky, D. E.; Cabelli, D.; Muckerman, J. T.; Fukushima, T.; Tanaka, K.; Fujita, E. *Inorg. Chem.* **2008**, *47*, 3958−3968. (i) Kimura, M.; Tanaka, K. *Angew. Chem., Int. Ed.* **2008**, *47*, 9768−9771. (j) Tannai, H.; Koizumi, T.; Wada, T.; Tanaka, K. *Angew. Chem., Int. Ed.* **2007**, *46*, 7112−7115. (k) Polyansky, D.; Cabelli, D.; Muckerman, J. T.; Fujita, E.; Koizumi, T.; Fukushima, T.; Wada, T.; Tanaka, K. *Angew. Chem., Int. Ed.* **2007**, *46*, 4169−4172. (l) Koizumi, T.; Tanaka, K. *Angew. Chem., Int. Ed.* **2005**, *44*, 5891−5894. (m) Tomon, T.; Koizumi, T.; Tanaka, K. *Angew. Chem., Int. Ed.* **2005**, *44*, 2229−2232. (n) Kobayashi, A.; Konno, H.; Sakamoto, K.; Sekine, A.; Ohashi, Y.; Iida, M.; Ishitani, O. *Chem.—Eur. J.* **2005**, *11*, 4219−4226. (o) Kobayashi, A.; Konno, H.; Sakamoto, K.; Sekine, A.; Ohashi, Y.; Iida, M.; Ishitani, O. *Chem.−Eur. J.* **2005**, *11*, 4219. (p) Fukuzumi, S.; Yuasa, J.; Satoh, N.; Suenobu, T. *J. Am. Chem. Soc.* **2004**, *126*, 7585. (q) Kobayashi, A.; Takatori, R.; Kikuchi, I.; Konno, H.; Sakamoto, K.; Ishitani, O. *Organometallics* **2001**, *20*, 3361−3363.

(5) (a) Padhi, S. K.; Tanaka, K. *Inorg. Chem.* **2011**, *50* (21), 10718−10723. (b) Padhi, S. K.; Kobayashi, K.; Masuno, S.; Tanaka, K. *Inorg. Chem.* **2011**, *50* (12), 5321−5323.

(6) (a) Stander-Grobler, E.; Schuster, O.; Heydenrych, G.; Cronje, S.; Tosh, E.; Albrecht, M.; Frenking, G.; Raubenheimer, H. G. *Organometallics* **2010**, *29*, 5821−5833. (b) Schuster, O.; Yang, L.; Raubenheimer, H. G.; Albrecht, B. *Chem. Rev.* **2009**, *109*, 3445−3478. (c) Raubenheimer, H. G.; Cronje, S. *Dalton Trans.* **2008**, 1265−1272. (d) Schuster, O.; Raubenheimer, H. G. *Inorg. Chem.* **2006**, *45*, 7997−7999. (e) Han, Y.; Huynh, H. V.; Tan, G. K. *Organometallics* **2007**, *26*, 6581−6585. (f) Iglesias-Sigüenza, J.; Ros, A.; Díez, E.; Alcarazo, M.; Álvarez, E.; Fernández, R.; Lassaletta, J. M. *Dalton Trans.* **2009**, 7113−7120. (g) Cabeza, J. A.; Del Río, I.; Goite, M. C.; Pérez-Carreño, E.; Pruneda, V. *Chem.—Eur. J.* **2009**, *15*, 7339−7349. (h) Song, G.; Zhang, Y.; Su, Y.; Deng, W.; Han, K.; Li, X. *Organometallics* **2008**, *27*, 6193−6201. (i) Cabeza, J. A.; del Río, I.; Pérez-Carreño, E.; Sánchez-Vega, M. G.; Vázquez-García, D. *Angew. Chem., Int. Ed.* **2009**, *48*, 555−558. (j) Cabeza, J. A.; del Río, I.; Pérez-Carreño, E.; Sánchez-Vega, M. G.; Vázquez-García, D. *Organometallics* **2010**, *29*, 4464−4471. (k) Cabeza, J. A.; del Río, I.; Pérez-Carreño, E.; Pruneda, V. *Chem.—Eur. J.* **2010**, *16*, 5425−5436. (l) Meyer, W. H.; Deetlefs, M.; Pohlmann, M.; Scholz, R.; Esterhuysen, M. W.; Julius, G. R.; Raubenheimer, H. G. *Dalton Trans.* **2004**, 413−420. (m) Esteruelas, M. A.; Fernández-Alvarez, F. J.; K.; Oñate, E. *Organometallics* **2007**, *26*, 5239−5245.

(7) (a) Gómez-Bujedo, S.; Alcarazo, M.; Pichon, C.; Alvarez, E.; Fernández, R.; Lassaletta, J. M. *Chem. Commun.* **2007**, 1180−1182. (b) Hahn, F. E.; Jahnke, M. C. *Angew. Chem., Int. Ed.* **2008**, *47*, 3122−3172.

(8) (a) Wiedemann, S. H.; Lewis, J. C.; Ellman, J. A.; Bergman, R. G. *J. Am. Chem. Soc.* **2006**, *128*, 2452. (b) Lewis, J. C.; Bergman, R. G.; Ellman, J. A. *J. Am. Chem. Soc.* **2007**, *129*, 5332. (c) Conejero, S.; Lara, P.; Paneque, M.; Petronilho, A.; Poveda, O.; Serrano, M. L.; Batiré, F.; Alvarez, E.; Moya, C.; Salazar, V.; Carmona, E. *Angew. Chem., Int. Ed.* **2008**, *47*, 4380−4383. (d) Alvarez, E.; Conejero, S.; Paneque, M.; Petronilho, A.; Poveda, O.; Serrano, M. L.; Carmona, E. *J. Am. Chem. Soc.* **2006**, *128*, 13060−13061. (e) Buil, M. L.; Esteruelas, M. A.; Garcés, K.; Oliván, M.; Oñate, E. *J. Am. Chem. Soc.* **2007**, *129*, 10998−10999.